# Thermal Conductivity of Si□N□ Ceramics Fabricated From Carbothermal-reduction-derived Powder

**Yuelong Wang**
University of Science and Technology Beijing
**Xingyu Li**
University of Science and Technology Beijing
**Haoyang Wu**
University of Science and Technology Beijing
**Baorui Jia**
University of Science and Technology Beijing
**Deyin Zhang**
University of Science and Technology Beijing
**Yiming Zhang**
University of Science and Technology Beijing
**Zhirui Zhang**
University of Science and Technology Beijing
**Jianjun Tian**
University of Science and Technology Beijing
**M.L. Qin** ( qinml@mater.ustb.edu.cn )
university of science and technology beijing
**Xuanhui Qu**
University of Science and Technology Beijing

**Rapid Communication**

**Keywords:** Carbothermal reduction, Si3N4 powder, low oxygen content, high thermal conductivity

**Posted Date:** September 22nd, 2021

**DOI:** https://doi.org/10.21203/rs.3.rs-910628/v1

# Abstract

$Si_3N_4$-based ceramic ($Si_3N_4$-5wt%$Y_2O_3$-3wt%MgO) was obtained from carbothermal-reduction-derived powder combined with gas pressure sintering. The phase, microstructure, thermal conductivity and mechanical properties of $Si_3N_4$ ceramics were comprehensively analyzed. Dense $Si_3N_4$ ceramic with uniform grain size was obtained after sintering at 1900°C for 7 h under a $N_2$ pressure of 1.2 MPa. The secondary phase consisted of $Y_4Si_2O_7N_2$ and $Y_2Si_3O_3N_4$ was found to gather around triangular grain boundaries. The thermal conductivity, flexural strength, hardness and fracture toughness of the $Si_3N_4$ ceramics were 95.7 $W{\cdot}m^{-1}{\cdot}k^{-1}$, 715 MPa, 17.2 GPa and 7.2 $MPa{\cdot}m^{1/2}$, respectively. The results were compared with product derived from commercial powder, the improvement of thermal conductivity (~8.3%) and fracture toughness (~4.3%) demonstrating the superiority of $Si_3N_4$ ceramics prepared from carbothermal-reduction-derived powder.


# Highlights

- A large fraction area of coarser grains (>1 μm) was obtained in $Si_3N_4$ ceramic.
- A narrow distribution of β-$Si_3N_4$ grain size was observed.
- The secondary phase gathered around triangular grain boundaries.
- Less secondary phase was due to low oxygen content in raw powder.

# 1. Introduction

Silicon nitride ($Si_3N_4$) ceramic is the key material for high power electronic device packaging, due to its high flexural strength and thermal conductivity[1–5]. $Si_3N_4$ has two common crystallographic modifications, α-$Si_3N_4$ and β-$Si_3N_4$, both exhibiting a hexagonal structure[2, 6]. Although Hirosaki et al.[7] reported that the theoretical thermal conductivity of β-$Si_3N_4$ along the a and c axes was 170 $W{\cdot}m^{-1}{\cdot}k^{-1}$ and 450 $W{\cdot}m^{-1}{\cdot}k^{-1}$. However, metallic impurity[8, 9], secondary phases[10–12] and lattice defects[13–16] have effects on thermal conductivity in polycrystalline $Si_3N_4$. The thermal conductivity of commercial $Si_3N_4$ ceramic substrate is less than 90 $W{\cdot}m^{-1}{\cdot}k^{-1}$. Therefore, high quality powder is highly desired to achieve excellent performance of $Si_3N_4$ ceramics.

There are three main methods for preparing $Si_3N_4$ powder in the market, including direct nitridation of silicon[17, 18], silicon-imide decomposition[19–21] and carbothermal reduction-nitridation method[22–25]. Carbothermal reduction method takes its advantage in large-scale applications due to its abundant sources of raw materials and low cost. Li et al.[26] used $C_6H_{12}O_6$ as carbon source to increase the mixing uniformity of silica and carbon, which would obtain high-purity α-$Si_3N_4$ with flocculent, granular and flake particle morphologies. Kang et al.[27] increased the α phase from 78–90% by adding 0.02 wt % $Si_3N_4$ seeds. In order to promote the nitriding reaction, nano-silica (20 nm) was often chosen as the raw material[22, 23, 25]. But the molten silica formed at high temperature hinders the process of reaction,

leading to agglomeration and higher β-$Si_3N_4$ content which deteriorate the properties of product. In our previous work[28], we developed a carbothermal reduction method to synthesize $Si_3N_4$ powder, where the spherical, monodisperse, 0.5 μm $SiO_2$ was selected as raw material. The $Si_3N_4$ powders with high α phase content, low metallic impurity content, regular morphology and good dispersivity were achieved. High performance of $Si_3N_4$ ceramics are expected to be obtained.

In previous studies, $Y_2O_3$ and MgO were generally used as sintering additives to prepare high thermal conductivity of $Si_3N_4$ ceramics[15, 29–31]. MgO can react with silica on the surface of $Si_3N_4$ particles or itself and form the liquid phase to promote densification at a low temperature[30, 32]. The rare earth oxides $Y_2O_3$ with high oxygen affinity can inhibit oxygen atoms occupying the substitutional position in $Si_3N_4$ lattice[31, 33, 34]. Zhou et al.[15] reported the highest thermal conductivity 177 $W{\cdot}m^{-1}{\cdot}k^{-1}$ of $Si_3N_4$ ceramic by SRBSN, holding at 1900°C for 60 h and cooling at a rate of 0.2°C/min. The sintering aids were $Y_2O_3$ and MgO composites. Axial pressure is often applied to assist the sintering, and is commonly practiced by hot press (HP) and spark plasma sintering (SPS). However, the axial pressure commonly leads to anisotropy of grain growth where β-$Si_3N_4$ is known as rod-like crystals, thus causing anisotropic properties of $Si_3N_4$ ceramic[6, 35, 36]. Kitayama et al.[36] prepared $Si_3N_4$ ceramics by hot press sintering (1800°C, 40 MPa pressure holding for 2 h) and heat treatment (1850°C, 1 MPa pressure holding for 16 h). It was found that the thermal conductivity parallel and perpendicular to the pressure direction were 72.3 $W{\cdot}m^{-1}{\cdot}k^{-1}$ and 94.9 $W{\cdot}m^{-1}{\cdot}k^{-1}$, respectively. Many studies also have shown the effect of texturing behaviors on the anisotropy of properties[37–40]. Moreover, these pressure-assisted methods offer very limited product geometry and the cost for processing scales up rapidly with product dimension. Gas pressure sintering is an effective solution to produce parts with complex shapes and isotropic properties[11, 12, 41–43], with the help of $N_2$ pressure of 1–10 MPa. Therefore, this method takes its advantages for widely fabricating $Si_3N_4$ ceramic substrates.

In this work, $Si_3N_4$ ceramic was prepared from carbothermal-reduction-derived powder combined with gas pressure sintering. 5 wt% $Y_2O_3$ and 3 wt% MgO were used as sintering additives. The thermal conductivity and mechanical properties of $Si_3N_4$ ceramics were analyzed. The results were compared with the product derived from commercial powder.

# 2. Experimental Procedure

Two types of $Si_3N_4$ materials were used for controlled experiments. One was a high-purity and monodisperse $Si_3N_4$ powder synthesized by carbothermal reduction method, named as SN1. The other was commercial $Si_3N_4$ powder (SN-E10; UBE Industries., Ltd., Japan) synthesized by silicon-imide decomposition method, named as SN2. The carbothermal reduction powder had been reported elsewhere[28]. SN1 powder was synthesized from $C/SiO_2$ = 3:1 at 1400°C, reaction time of 6 h and nitrogen flow rate of 800 ml/min. The impurity content of the two $Si_3N_4$ powder is showed in Table 1. The

sintering aids were $Y_2O_3$ (purity > 99.99 wt%, Meryer Chemical Technology Co., Ltd., China) and MgO (purity > 99.99 wt%, Aladdin Industrial Co., Ltd., China).

Table 1
Impurity content of Silicon Nitride powders.

| Sample | O (wt%) | Fe (ppm) | Al (ppm) | Ca (ppm) | Cl (ppm) |
|---|---|---|---|---|---|
| SN1 | 0.85 | 14 | 23 | 16 | - |
| SN2 | 1.23 | 10 | 1 | < 1 | < 100 |
| "-": not detected | | | | | |

The average particle size was measured by the laser scattering method (LMS-30, Seishin Enterprise Co. Ltd, Japan). The specific surface area of the two $Si_3N_4$ powders was analyzed by the BET method (QUADRASORB SIMP, Quanta chrome Instruments, Florida, America). The relative phase content of powder was calculated using X-ray techniques, according Eq. (1). The physical properties of the two $Si_3N_4$ powders are shown in Table 2.

Table 2
Physical properties of Silicon Nitride powders.

| Sample | α (wt%) | Specific Surface Area ($m^2/g$) | $D_{50}$ (μm) |
|---|---|---|---|
| SN1 | ≥99 | 3.74 | 0.57 |
| SN2 | ≥95 | 10.55 | 0.83 |

$$\alpha\% = \frac{I_{\alpha(101)} + I_{\alpha(201)}}{I_{\alpha(101)} + I_{\alpha(201)} + I_{\beta(200)} + I_{\beta(101)}}$$

1

The starting powders were mixed according to the mass ratio of $Si_3N_4$: $Y_2O_3$: MgO = 92:5:3. Mixtures were homogenized in a plastic bottle at 80 rpm for 10 h with 3 wt% stearic acid as dispersant and ethanol as solvent. The pulp was dried in vacuum at 80°C for 5 h and sieving through a 100-mesh screen. Powder mixture was uniaxially pressed in a stainless die and then cold isostatically pressed at 200 MPa for 15 min. The samples were sintered at 1900°C for 7 h under a $N_2$ pressure of 1.2 MPa, in a tungsten crucible with a high-purity BN plate at the bottom.

The bulk density (ρ) was measured by the Archimedes method. X-ray diffraction (XRD, Rigaku, D/max-RB12) with Cu Ka radiation was used for phase characterization. The powder morphology and ceramic microstructure were observed using field-emission scanning electron microscope (FE-SEM, ZEISS ULTRA 55), and the surface was coated with gold for 120 s. Oxygen content was measured by a N and O content

tester (ON-3000). The flexural strength of sintered samples (4 × 3 × 36 mm) was tested by three-point bending method (Instron, Model 1185, Canton, USA). Fracture toughness was evaluated by single-edge notched beam method after a V-shaped notch with a crack depth of 2 mm was introduced into the 3 mm × 36 mm surface. The thermal conductivity of sintered materials was calculated using the formula $k = \rho C_p \alpha$, where ρ, $C_p$, and α are density, heat capacity, and thermal diffusion coefficient of $Si_3N_4$, respectively. The thermal diffusivity (α) was measured by the laser-flash method (LFA 447, NETZSCH, Germany). The specific heat capacity ($C_p$) of all $Si_3N_4$ samples was taken as 0.68 $J \cdot g^{-1} \cdot K^{-1}$ in this work.

# 3. Results And Discussion

Figure 1 shows that pure $Si_3N_4$ phases dominate the XRD profile for both two powders and they all have a high content of α phase. However, the two $Si_3N_4$ powders have significant disparity in their morphology, as shown in Fig. 2. While SN2 sample exhibits typical agglomeration with fine $Si_3N_4$ particles (100–200 nm), SN1 sample exhibits $Si_3N_4$ particles with improved dispersivity and near spherical shape. The average particle size is 0.57 μm and 0.83 μm for SN1 and SN2, respectively. The specific surface area (SSA) of SN1 and SN2 is 3.74 $m^2/g$ and 10.55 $m^2/g$, respectively. Therefore, SN2 sample will be expected to yield better sintering activity, because its larger SSA indicates higher free surface energy, i.e., larger driven force for sintering[44, 45]. The difference properties of $Si_3N_4$ ceramics obtained from SN1 and SN2 powder was introduced in below.

XRD patterns in Fig. 3 show the phase evolution of the two $Si_3N_4$ samples at the sintering stage. It shows that β-$Si_3N_4$ completely replaces the α-$Si_3N_4$ and secondary phase ($Y_4Si_2O_7N_2$ and $Y_2Si_3O_3N_4$) forms after gas pressure sintering at 1900°C for 7 h under a $N_2$ pressure of 1.2 MPa. Note that the grain size and spatial distribution of secondary phase of the two sintered $Si_3N_4$ samples are very different, as shown in Fig. 4. Both $Si_3N_4$ ceramics have typical bimodal microstructures with elongated grains embedded in a matrix of finer grains. Furthermore, Fig. 5 illustrated that the grain diameter distribution of SN1-5-3 sample was more uniform than SN2-5-3. The median grain diameters ($D_{50}$) were 2.4 μm and 1.7 μm for SN1-5-3 and SN2-5-3 samples, respectively. In SN1-5-3 sample, there are a large fraction area of coarser grains (> 1 μm) and a narrow distribution of grain size. The secondary phase gathers around triangular grain boundaries. However, some larger elongated grains were detected in SN2-5-3 sample. And the secondary phases spread over finer grains which are in the majority. Agglomeration and higher sintering activity of SN2 powder promotes abnormal grain growth. Less secondary phase in the SN1-5-3 sample (7.21 vol%) could be attributed the lower oxygen content in SN1 powder. Moreover, the density of SN1-5-3 ceramic is slightly lower than that of SN2-5-3, which are 3.18 $g \cdot cm^{-3}$ and 3.20 $g \cdot cm^{-3}$, respectively (Table 3).

Table 3
Bulk density, Oxygen content and Thermal Conductivity of the SN1-5-3 and SN2-5-3 sample.

| Sample | Density ($g \cdot cm^{-3}$) | Grain-boundary Volume fraction (vol%) | Oxygen content (wt%) | Thermal Conductivity ($W \cdot m^{-1} \cdot K^{-1}$) |
|---|---|---|---|---|
| SN1-5-3 | 3.18 | 7.21 | 1.75 | 95.7 |
| SN2-5-3 | 3.20 | 7.57 | 2.01 | 88.4 |

The thermal conductivity of the two sintered samples are 95.7 and 88.4 $W \cdot m^{-1} \cdot k^{-1}$, respectively (Table 3). Three main factors influence the thermal conductivity of $Si_3N_4$ ceramics. Firstly, the thermal conductivity of the secondary phase is generally low, only 1–10 $W \cdot m^{-1} \cdot k^{-1}$, and the presence of a large amount of the secondary phase often has harmful effect on the thermal conductivity of $Si_3N_4$ ceramic[11, 15, 29, 43]. Wasanapiarnpong et al.[46] showed that thermal conductivity of $Si_3N_4$ ceramics increased from 44 to 89 $W \cdot m^{-1} \cdot k^{-1}$ by the decrease in glassy phase after heat-treatment at 2223 K for 8 h under a nitrogen gas pressure of 1.0 MPa. And the improvement of thermal conductivity (~ 25.5%) was obtained from carbothermal reduction of oxynitride secondary phase[16]. Therefore, less volume fraction of secondary phases would increase $Si_3N_4$-$Si_3N_4$ grains contiguity which are favorable to thermal conductivity. The grain-boundary volume fraction in SN1-5-3 and SN2-5-3 samples were 7.21 vol% and 7.57 vol%, respectively. Secondly, grain structure has great influence on thermal conductivity. Kitayama et al.[36] reported that grain growth alone does not significantly improve the thermal conductivity of β-$Si_3N_4$ once grain size reaches a certain value (~ 1 μm). The proportion of larger grains (> 1 μm) is a key factor in determining the thermal conductivity of $Si_3N_4$ ceramics. The area fraction (AF) of fine grains (d < 1 μm) in SN1-5-3 and SN2-5-3 samples were 8.3% and 21.5%, respectively, indicating more fine grains observed in SN2-5-3 sample decrease thermal conductivity. Thirdly, note that the content of oxygen impurity in SN2 powder is higher than SN1. Oxygen would dissolve in the $Si_3N_4$ lattice with the formation of Si vacancies which would reduce the phonon mean free path, and then decrease the thermal conductivity[14, 15, 47]. Besides, the oxygen content of SN1-5-3 and SN2-5-3 samples is 1.75 wt% and 2.01 wt%, respectively (Table 3). Benefiting from alleviating those unfavorable effects, the thermal conductivity of SN1-5-3 sample is about 8.3% higher than that of SN2-5-3 sample.

Figure 6 gives the flexural strength and hardness of two sintered ceramics. The difference in hardness between SN1-5-3 and SN2-5-3 was relatively small, which were 17.2 GPa and 16.8 GPa, respectively. A lower average value of flexural strength was measured for SN1-5-3 (715 MPa) than for SN2-5-3 (753 MPa), due to the absence of extremely large elongated grains[48, 49]. The elongated β-$Si_3N_4$ grains grow to form an interlocking microstructure, leading to high strength and toughness of $Si_3N_4$ ceramic. In addition, the toughness of the SN1-5-3 and SN2-5-3 sample reached 7.2 $MPa \cdot m^{1/2}$ and 6.9 $MPa \cdot m^{1/2}$.

# 4. Conclusion

In this study, two kinds of $Si_3N_4$-based ceramics were prepared by gas pressure sintering: one using carbothermal-reduction-derived powder and another using commercial powder. Benefiting from less oxygen and metallic impurity content, carbothermal-reduction-derived powders were sintered to obtain better thermal conductivity of $Si_3N_4$ ceramics. Major finer grains and some larger elongated β-$Si_3N_4$ grains were detected in ceramic prepared from commercial powder with high sintering activity. While, a large fraction area of coarser grains (> 1 μm) achieved from carbothermal reduction powder. As a result, the thermal conductivity, flexural strength, hardness and toughness of the $Si_3N_4$ ceramics were 95.7 $W \cdot m^{-1} \cdot k^{-1}$, 715 MPa, 17.2 GPa and 7.2 $MPa \cdot m^{1/2}$, respectively. $Si_3N_4$ ceramics with high strength and thermal conductivity could be prepared from carbothermal-reduction-derived powder.

## Declarations

# Acknowledgments

This work is financially supported by the National Natural Science Foundation Program of China (51774035, 51604025, 51574031, 51574030, 51574029 and 51604240), Key Research and Development Project of Hebei Province (No.20311001D), the Natural Science Foundation Program of Beijing (2202031, 2174079 and 2162027), the Fundamental Research Funds for the Central Universities (FRF-TP-19-015A3, FRF-TP-19-003C2 and FRF-TP-17-034A2), USTB-NTUT Joint Research Program (06310061), the Scientific Research Foundation of Hunan Provincial Education Department (18A196) and the Postdoctor Research Foundation of Shunde Graduate School of University of Science and Technology Beijing (2020BH014).

## References

[1] Katz RN. Applications of Silicon Nitride Based Ceramics in the U.S. *Mat. Res. Soc. Symp. Proc* 1997, **287**: 197-208.

[2] Riley FL. Silicon Nitride and Related Materials. *J. Am. Ceram. Soc* 2000, **83**: 245-265.

[3] Okada A. Automotive and industrial applications of structural ceramics in Japan. *J. Eur. Ceram. Soc.* 2008, **28**: 1097-1104.

[4] Xiang H, Feng Z, Li Z*, et al.* Theoretical predicted high-thermal-conductivity cubic $Si_3N_4$ and $Ge_3N_4$: promising substrate materials for high-power electronic devices. *Scientific reports* 2018, **8**: 14374.

[5] Hu F, Xie ZP, Zhang J*, et al.* Promising high-thermal-conductivity substrate material for high-power electronic device: silicon nitride ceramics. *Rare Metals* 2020, **39**: 463-478.

[6] Kitayama M, Hirao K, Toriyama M*, et al.* Modeling and simulation of grain growth in $Si_3N_4$ - anisotropic Ostwald ripening. *Acta Mater.* 1998, **46**: 6541-6550.

[7] Hirosaki N, Ogata S, Kocer C*, et al.* Molecular dynamics calculation of the ideal thermal conductivity of single-crystal α- and β-$Si_3N_4$. *Phys. Rev. B* 2002, **65**: 1-11.

[8] Kusano D, Noda Y, Shibasaki H*, et al.* Effects of Impurity Iron Content on Characteristics of Sintered Reaction-Bonded Silicon Nitride. *Int. J. Appl. Ceram. Tec.* 2013, **10**: 690-700.

[9] Kusano D, Hyuga H, Zhou Y*, et al.* Effect of Aluminum Content on Mechanical Properties and Thermal Conductivities of Sintered Reaction-Bonded Silicon Nitride. *Int. J. Appl. Ceram. Tec.* 2014, **11**: 534-542.

[10] Lee HM, Lee EB, Kim DL*, et al.* Comparative study of oxide and non-oxide additives in high thermal conductive and high strength $Si_3N_4$ ceramics. *Ceram. Int.* 2016, **42**: 17466-17471.

[11] Hu F, Zhu TB, Xie ZP*, et al.* Elimination of grain boundaries and its effect on the properties of silicon nitride ceramics. *Ceram. Int.* 2020, **46**: 12606-12612.

[12] Wang WD, Yao DX, Liang HQ*, et al.* Novel silicothermic reduction method to obtain $Si_3N_4$ ceramics with enhanced thermal conductivity and fracture toughness. *J. Eur. Ceram. Soc.* 2020, **41**: 1735-1738.

[13] Hirao K, Tsuge A, Toriyama M*, et al.* Oxygen Content in β-$Si_3N_4$ Crystal Lattice. *J. Am. Ceram. Soc* 1999, **82**: 3263-3265.

[14] Kitayama M, Hirao K, Tsuge A*, et al.* Thermal Conductivity of β-$Si_3N_4$: II, Effect of Lattice Oxygen. *J. Am. Ceram. Soc* 2000, **83**: 1985-1992.

[15] Zhou Y, Hyuga H, Kusano D*, et al.* A tough silicon nitride ceramic with high thermal conductivity. *Adv. Mater.* 2011, **23**: 4563-4567.

[16] Li YS, Kim H-N, Wu HB*, et al.* Enhanced thermal conductivity in $Si_3N_4$ ceramic by addition of a small amount of carbon. *J. Eur. Ceram. Soc.* 2019, **39**: 157-164.

[17] Itoh T. Preparation of pure α-silicon nitride from silicon powder. *J. Mater. Sci. Lett.* 1990, **9**: 19-20.

[18] Jin X, Xing PF, Zhuang YX*, et al.* Effect of $Si_3N_4$ diluent on direct nitridation of silicon powder. *Ceram. Int.* 2019, **45**: 10943-10950.

[19] Mazdiyasni KS, Cooke CM. Synthesis, Characterization, and Consolidation of $Si_3N_4$ Obtained from Ammonolysis of $SiCl_4$. *J. Am. Ceram. Soc.* 1973, **56**: 628-633.

[20] Yamada T, Kawahito T, Iwai T. Crystallization of amorphous $Si_3N_4$ prepared by the thermal decomposition of $Si(NH)_2$. *J. Mater. Sci. Lett.* 1983, **2**: 275-278.

[21] Chung YK, Koo JH, Kim SA*, et al.* Optimization of reaction parameters for synthesis of amorphous silicon nitride powder by vapor phase reaction. *Ceram. Int.* 2014, **40**: 14563-14568.

[22] Komeya K, Inoue H. Synthesis of the α form of silicon nitride from silica. *J. Mater. Sci. Lett.* 1975, **7**: 1243-1246.

[23] Zhang S-C, Cannon WR. Preparation of Silicon Nitride from Silica. *J. Am. Ceram. Soc* 1984, **67**: 691-695.

[24] Dijien FKv, Vogt U. The chemistry of the carbothermal synthesis of α-$Si_3N_4$: Reaction mechanism, reaction rate and properties of the product. *J. Eur. Ceram. Soc.* 1992, **10**: 273-282.

[25] Koc R, Kaza S. Synthesis of α-$S_3N_4$ from Carbon Coated Silica by Carbothermal Reduction and Nitridation. *J. Eur. Ceram. Soc.* 1998, **18**: 1471-1477.

[26] Li B, Feng YY, Li GQ*, et al.* Preparation of high-purity α-$Si_3N_4$ nano-powder by precursor-carbothermal reduction and nitridation. *Ceram. Int.* 2019, **45**: 6335-6339.

[27] Kang I-H, Komeya K, Meguro T*, et al.* Preparation of $Si_3N_4$ Powder from the System $SiO_2$-C-$N_2$ with $Si_3N_4$ Seed. *J. Ceram. Soc. Jpn.* 1998, **106**: 30-34.

[28] Wang YL, Wu HY, Jia BR*, et al.* Synthesis of monodisperse and high-purity α-$Si_3N_4$ powder by carbothermal reduction and nitridation. *Adv. Powder Technol.* 2021.

[29] Liu W, Tong WX, He RX*, et al.* Effect of the $Y_2O_3$ additive concentration on the properties of a silicon nitride ceramic substrate. *Ceram. Int.* 2016, **42**: 18641-18647.

[30] Go S-I, Li YS, Ko J-W*, et al.* Microstructure and Thermal Conductivity of Sintered Reaction-Bonded Silicon Nitride: The Particle Size Effects of MgO Additive. *Adv. Mater. Sci. Eng.* 2018, **2018**: 1-5.

[31] Zhou Y, Hyuga H, Kusano D*, et al.* Effects of yttria and magnesia on densification and thermal conductivity of sintered reaction-bonded silicon nitrides. *J. Am. Ceram. Soc* 2019, **102**: 1579-1588.

[32] Lange FF. Phase Relations in the System $Si_3N_4$-$SiO_2$-MgO and Their Interrelation with Strength and Oxidation. *J. Am. Ceram. Soc* 1977, **61**: 53-56.

[33] Negita K. Ionic Radii and Electronegativities of Effective Sintering Aids for $Si_3N_4$ Ceramics. *J. Mater. Sci. Lett.* 1985, **4**: 417-418.

[34] Kitayama M, Hirao K, Watari K*, et al.* Thermal Conductivity of β-$Si_3N_4$ : III, Effect of Rare-Earth (RE=La,Nd,Gd,Y,Yb,and Sc) Oxide Additives. *J. Am. Ceram. Soc* 2001, **84**: 353-358.

[35] Hirao K, Watari K, Brito ME*, et al.* High Thermal Conductivity in Silicon Nitride with Anisotropie Microstructure. *J. Am. Ceram. Soc* 1996, **79**.

[36] Kitayama M, Hirao K, Toriyama M*, et al.* Thermal Conductivity of β-$Si_3N_4$: I, Effects of Various Microstructural Factors. *J. Am. Ceram. Soc* 1999, **82**: 3105-3112.

[37] Zhu XW, Suzuki TS, Uchikoshi T*, et al.* Texture Development in $Si_3N_4$ Ceramics by Magnetic Field Alignment during Slip Casting. *J. Ceram. Soc. Jpn.* 2006, **114**: 979-987.

[38] Zhu XW, Suzuki TS, Uchikoshi T*, et al.* Texturing behavior in sintered reaction-bonded silicon nitride via strong magnetic field alignment. *J. Eur. Ceram. Soc.* 2008, **28**: 929-934.

[39] Zhu XW, Sakka Y, Suzuki TS*, et al.* The c-axis texturing of seeded $Si_3N_4$ with β-$Si_3N_4$ whiskers by slip casting in a rotating magnetic field. *Acta Mater.* 2010, **58**: 146-161.

[40] Zhu XW, Sakka Y, Zhou Y*, et al.* A strategy for fabricating textured silicon nitride with enhanced thermal conductivity. *J. Eur. Ceram. Soc.* 2014, **34**: 2585-2589.

[41] Wang ZH, Bai B, Ning XS. Effect of rare earth additives on properties of silicon nitride ceramics. *Advances in Applied Ceramics* 2014, **113**: 173-177.

[42] Liu W, Tong WX, Lu XX*, et al.* Effects of different types of rare earth oxide additives on the properties of silicon nitride ceramic substrates. *Ceram. Int.* 2019, **45**: 12436-12442.

[43] Wang WD, Yao DX, Liang HQ*, et al.* Effect of in-situ formed $Y_2O_3$ by metal hydride reduction reaction on thermal conductivity of β-$Si_3N_4$ ceramics. *J. Eur. Ceram. Soc.* 2020, **40**: 5316-5323.

[44] Karakuş N, Osman Kurt A, Duran C*, et al.* Sintering behaviour of silicon nitride powders produced by carbothermal reduction and nitridation. *Adv. Powder Technol.* 2013, **24**: 697-702.

[45] Dong H, Zhao Z, Wang C. Effect of powder characteristics on the thermal conductivity and mechanical properties of $Si_3N_4$ ceramics sintered by Spark plasma sintering. *Journal of Materials Science: Materials in Electronics* 2019, **30**: 7590-7599.

[46] Wasanapiarnpong T, Wada S, Imai M*, et al.* Effect of post-sintering heat-treatment on thermal and mechanical properties of $Si_3N_4$ ceramics sintered with different additives. *J. Eur. Ceram. Soc.* 2006, **26**: 3467-3475.

[47] Yokota H, Abe H, Ibukiyama M. Effect of lattice defects on the thermal conductivity of β-$Si_3N_4$. *J. Eur. Ceram. Soc.* 2003, **23**: 1751-1759.

[48] Thompson D. Tough cookery. *Nature* 1997, **389**: 675-676.

[49] Pablos AD, Bermudo J, Osendi MI. Microstructure and Mechanical Properties of Silicon Nitride Materials Fabricated from SHS Powders. *J. Am. Ceram. Soc.* 2001, **84**: 1033-1036.

# Figures

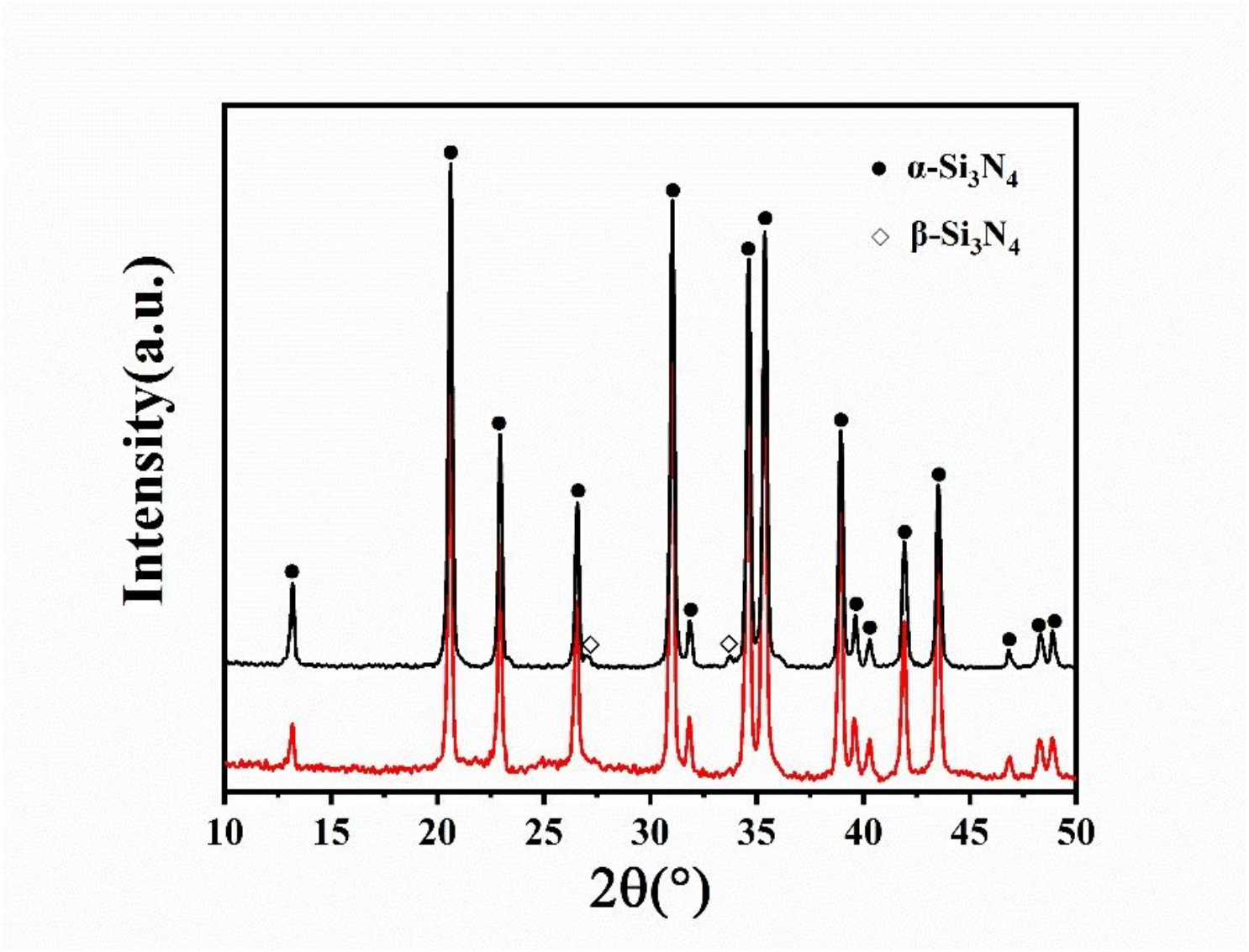


Figure 1

XRD patterns of two Si3N4 powders.

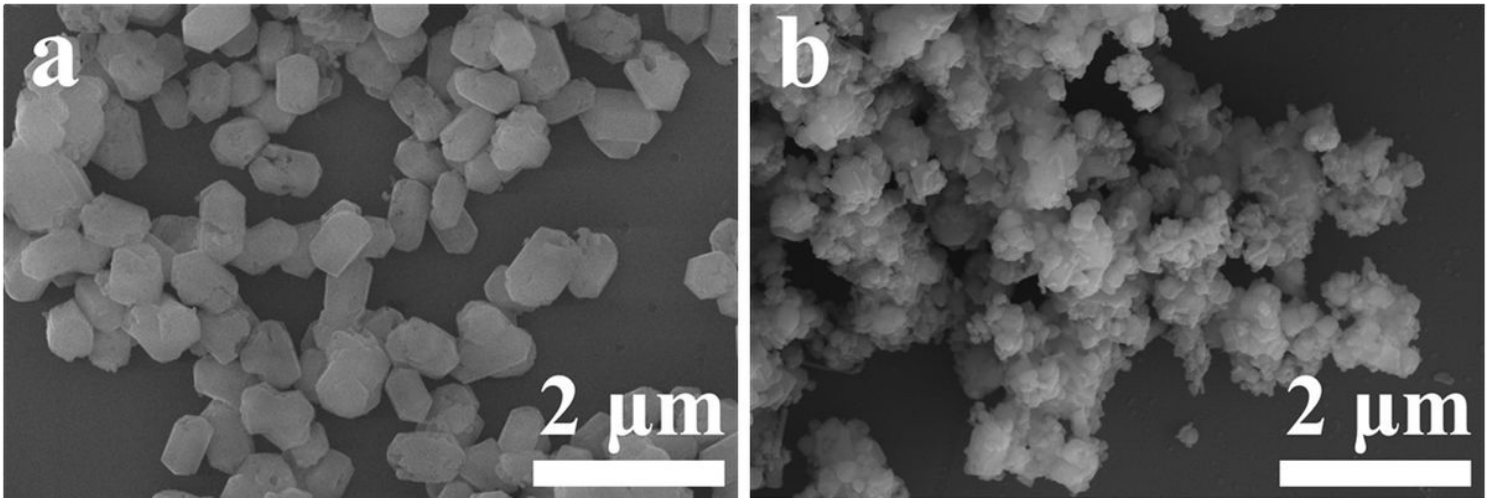


Figure 2

SEM images of Si3N4 powders: (a) SN1, (b) SN2.

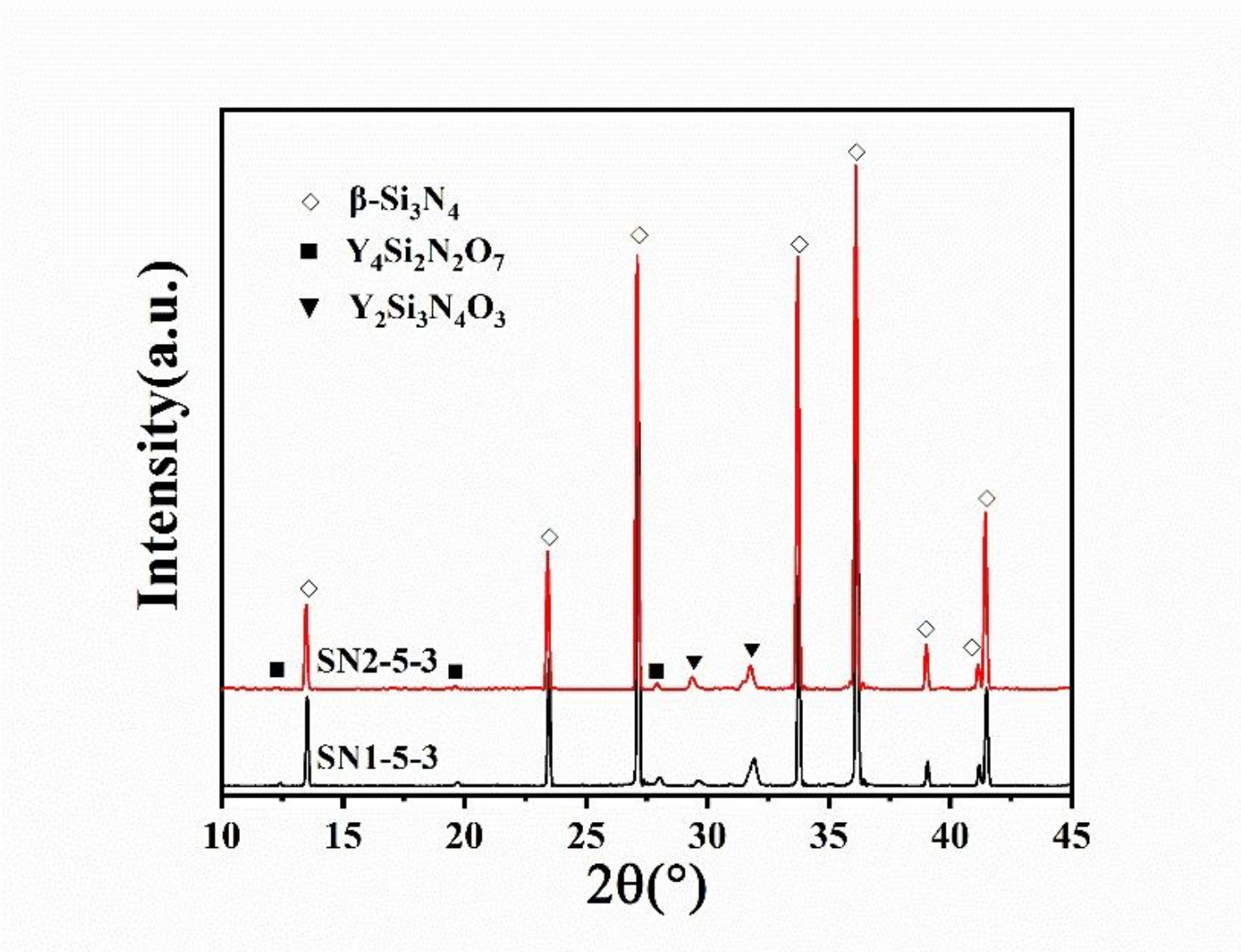


**Figure 3**

XRD patterns of the sintered materials.

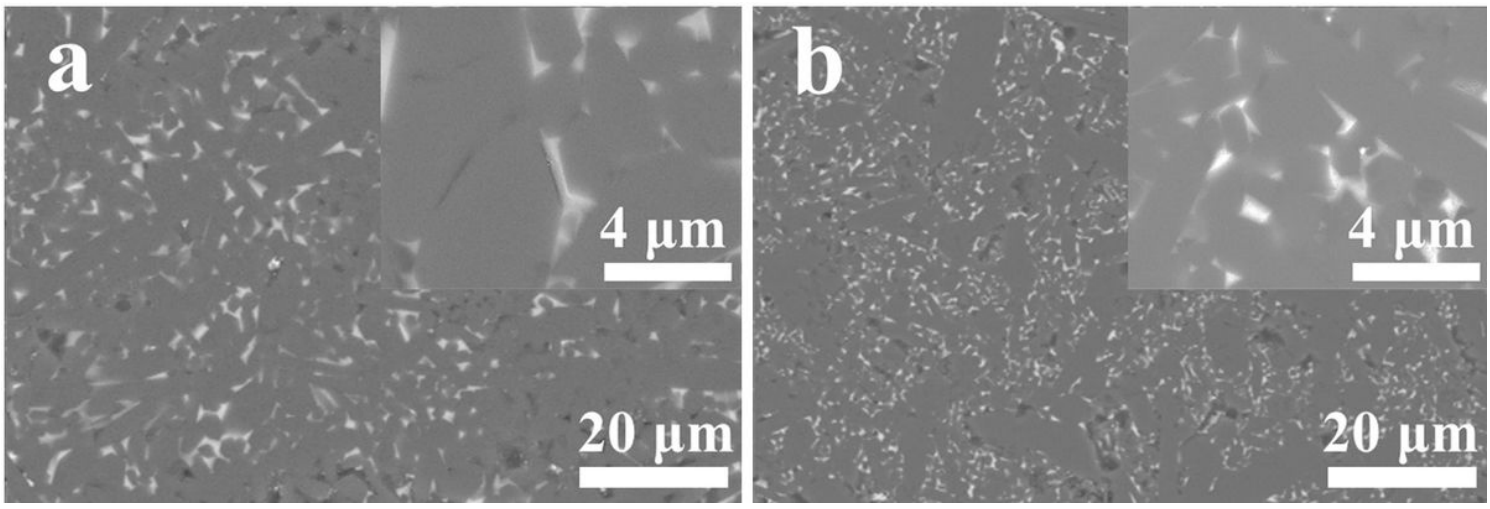

## Figure 4

SEM images of polished surfaces of (a) SN1-5-3 and (b) SN2-5-3.

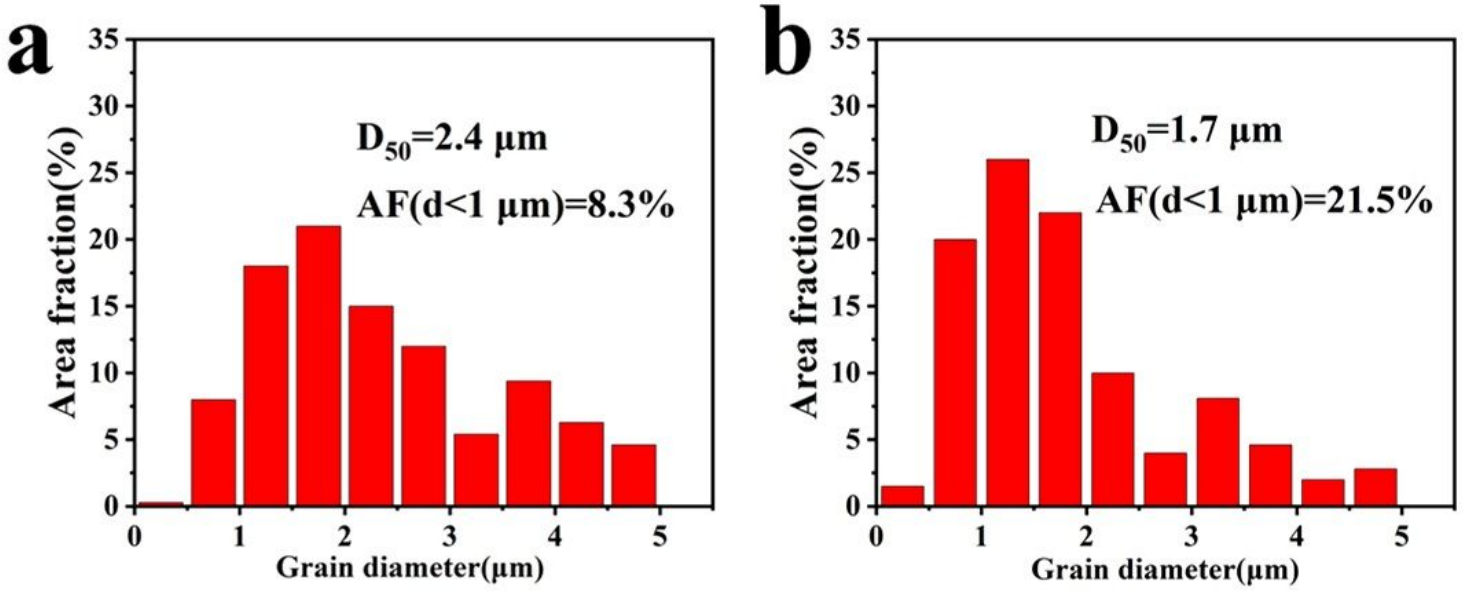


## Figure 5

Histograms of grain diameter distributions of (a) SN1-5-3 and (b) SN2-5-3.

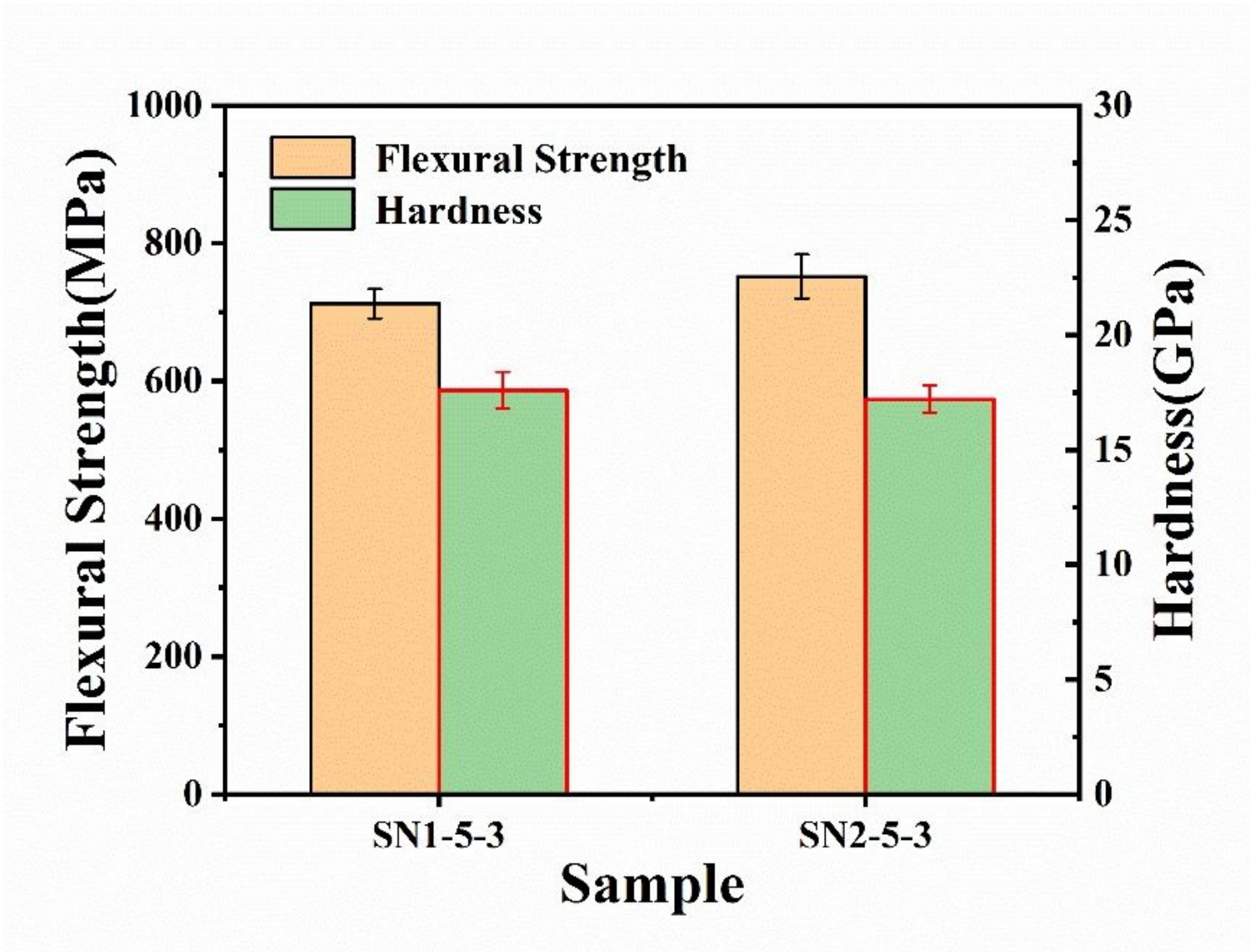


**Figure 6**

Flexural strength and Hardness of the sintered materials.